Determination of Single Particle Mass Spectral Signatures from Light-Duty Vehicle Emissions

ARTICLE *in* ENVIRONMENTAL SCIENCE AND TECHNOLOGY · JULY 2005

Impact Factor: 5.33 · DOI: 10.1021/es0489947 · Source: PubMed

3 AUTHORS, INCLUDING:

Kim Prather
University of California, San Diego
297 PUBLICATIONS **9,851** CITATIONS

SEE PROFILE

Determination of Single Particle Mass Spectral Signatures from Light-Duty Vehicle Emissions

DAVID A. SODEMAN, STEPHEN M. TONER, AND KIMBERLY A. PRATHER*

Department of Chemistry and Biochemistry, Scripps Institution of Oceanography, University of California, San Diego, La Jolla, California 92093-0314

In this study, 28 light-duty gasoline vehicles (LDV) were operated on a chassis dynamometer at the California Air Resources Board Haagen-Smit Facility in El Monte, CA. The mass spectra of individual particles emitted from these vehicles were measured using aerosol time-of-flight mass spectrometry (ATOFMS). A primary goal of this study involves determining representative size-resolved single particle mass spectral signatures that can be used in future ambient particulate matter source apportionment studies. Different cycles were used to simulate urban driving conditions including the federal testing procedure (FTP), unified cycle (UC), and the correction cycle (CC). The vehicles were selected to span a range of catalytic converter (three-way, oxidation, and no catalysts) and engine technologies (vehicles models from 1953 to 2003). Exhaust particles were sampled directly from a dilution and residence chamber system using particle sizing instruments and an ATOFMS equipped with an aerodynamic lens (UF-ATOFMS) analyzing particles between 50 and 300 nm. On the basis of chemical composition, 10 unique chemical types describe the majority of the particles with distinct size and temporal characteristics. In the ultrafine size range (between 50 and 100 nm), three elemental carbon (EC) particle types dominated, all showing distinct EC signatures combined with Ca, phosphate, sulfate, and a lower abundance of organic carbon (OC). The relative fraction of EC particle types decreased as particle size increased with OC particles becoming more prevalent above 100 nm. Depending on the vehicle and cycle, several distinct OC particle types produced distinct ion patterns, including substituted aromatic compounds and polycyclic aromatic hydrocarbons (PAH), coupled with other chemical species including ammonium, EC, nitrate, sulfate, phosphate, V, and Ca. The most likely source of the Ca and phosphate in the particles is attributed to the lubricating oil. Significant variability was observed in the chemical composition of particles emitted within the different car categories as well as for the same car operating under different driving conditions. Two-minute temporal resolution measurements provide information on the chemical classes as they evolved during the FTP cycle. The first two minutes of the cold start produced more than 5 times the number of particles than any other portion of the cycle, with one class of ultrafine particles (EC coupled with Ca, OC, and phosphate) preferentially produced. By number, the three EC with Ca classes (which also contained OC, phosphate, and sulfate) were the most abundant classes produced by the nonsmoking vehicles. The smoker category produced the highest number of particles, with the dominant classes being OC comprised of substituted monoaromatic compounds and PAHs, coupled with Ca and phosphate, thus suggesting used lubricating oil was associated with many of these particles. These studies show, by number, EC particles dominate gasoline emissions in the ultrafine size range particularly for the lowest emitting newer vehicles, suggesting the EC signature alone cannot be used as a unique tracer for diesels. This represents the first report of high time- and size-resolved chemical composition data showing the mixing state of nonrefractory elements in particles such as EC for vehicle emissions during dynamometer source testing.

* Corresponding author phone: (858)822-5312; fax: (858)534-7042; e-mail: kprather@ucsd.edu.

Introduction

Vehicle emissions strongly affect the air quality of California. It has been reported that 65% or more of air pollution in the South Coast Air Basin in California can be attributed to vehicular emissions (*1*−*4*). These emissions contribute to poor visibility and high particulate matter (PM) in the basin (*5*, *6*). Concern over correlations between particulate matter and adverse health effects (*7*−*9*) results in vehicular emissions being a significant area of focus in relation to the overall health of the basin's population. With an estimated population of 16 million people in the South Coast Air Basin and the poor air quality in the region, the California Air Resources Board (CARB) has introduced more stringent regulations on the emissions from gasoline-fueled vehicles (*10*). To achieve these stricter standards, efforts have shifted toward the development of newer catalytic converter technology and the introduction of reformulated gasoline.

The majority of source characterization and apportionment studies have traditionally used filter-based measurements (*11*−*19*). Such studies perform elemental analysis on the filter samples that can be used for source apportionment using chemical mass balance methods. When there are no unique elemental tracers (i.e., meat cooking, secondary organic aerosols), researchers often shift their focus to identifying unique organic source tracers. Some organic compounds can undergo chemical reactions in the atmosphere, losing their original signature, while others, such as hopanes and steranes, are less reactive and retain their identities (*20*). As a result of these challenges, there is some debate regarding which sources make the largest contributions to ambient particulate matter. Ambient apportionment studies performed in different locations have shown significantly different PM apportionment results, which could be due to the different sampling locations, PM sampling, and characterization methods, or apportionment methodologies used in these studies (*21*). In an effort to learn more about ambient PM sources, newer approaches are now being used for source apportionment to complement filter studies which perform online analysis of aerosol composition (*22*−*27*). Many of these methods fragment the organic compounds in the particles (*28*−*30*), making speciation of some individual organic compounds difficult. The fragmentation patterns can be used for identifying general classes of organic species (*31*, *32*). Also, different ionization methods are being used which reduce the degree of fragmentation (*33*−*36*). Single particle

mass spectrometry (SPMS) techniques are used to measure chemical "fingerprints". Thus, the goal of most SPMS studies is not to identify each organic compound but instead to determine unique chemical signatures on the basis of the combinations of species in the single particle mass spectra that can ultimately be used for source apportionment (*37*). The chemical classes presented herein will ultimately be utilized in source apportionment studies in several different ways. The first will involve a univariate approach, where an ambient particle with a specific signature will be assigned to a specific source if the particle signature closely matches a given source particle class. The particles assigned to each type will be summed and the number concentrations of ambient particles from different sources derived. By assuming particle densities, these number concentrations can be converted to mass concentrations. The second approach will use multivariate analysis to match ambient particles to sources on the basis of temporal trends and the statistics of all ambient signatures present at any given time (*38*, *39*). The third level of analysis will involve a combined approach where simultaneous measurements will be made using a suite of techniques including ATOFMS, gas phase, particle phase, traffic counts, and meteorological data (i.e., VOCs, CO, NO_x, and PM absorption) to assign the ambient particles to specific sources. Ultimately, these results will be compared with traditional filter-based source apportionment with the goal of better understanding PM sources. This final approach has the strongest potential for providing detailed source apportionment. This paper focuses on the major particle types emitted from light-duty vehicles (LDVs) and discusses the variability of these classes for different vehicles and cycles. We have found the particle signatures measured in this study are indeed representative of those sampled during ambient studies. Another paper describes utilizing these signatures to identify particles types from LDV and heavy-duty vehicles in ambient air (*40*).

The study described herein is part of a series of studies being conducted in our laboratory characterizing combustion sources with SPMS (*41*−*45*). This study investigates the aerodynamic size and chemical composition of particles emitted from a range of LDVs and cycles with the goal of producing a broad range of single particle signatures that can be used for ambient apportionment studies. ATOFMS is used to characterize PM from low-emission vehicles (LEV), three-way catalyst (TWC), oxidation catalyst (oxy-cat), and noncatalyst equipped vehicles (noncat), as well as vehicles emitting visible amounts of blue smoke (smoker) which signifies oil emissions. Size-resolved composition information is presented for particles ranging in size between 50 and 180 nm. This represents the first report of high time- and size-resolved composition data showing the mixing state of nonrefractory elements such as EC in individual particles produced by vehicle emissions during dynamometer source testing.

Experimental Section

Twenty-eight light LDVs were tested on a chassis dynamometer at the California Air Resources Board Haagen-Smit Laboratory in El Monte, California. The make, model, year, and mileage as well as catalytic converter category of each of the vehicles tested are listed in Table S1, located in the supplemental information section. These vehicles span a wide range of different exhaust technologies and production years. Two of the vehicles produced excessive visible emissions and thus were classified as smokers. The remaining vehicles had the following catalytic converter types: no catalyst (2 vehicles), oxidation catalyst (3 vehicles), three-way catalyst (11 vehicles), and low-emission vehicles (LEV, three-way catalyst with emissions control) (10 vehicles). Also included in Table S1 are the cycles that each vehicle was driven through. Each of these vehicles was tested under one or more of the following cycles: federal test procedure (FTP), unified cycle (UC), and correction cycle (CC). A brief description of the cycles is given below. The emissions from the tailpipe traveled through a constant volume sampler into a dilution and residence chamber setup (*46*, *47*) before being sampled with the following instrumentation: a scanning mobility particle sizer (SMPS TSI model 3081 electrostatic classifier and TSI model 3010 condensation particle counter) and an ultrafine aerosol time-of-flight mass spectrometer (UF-ATOFMS). The UF-ATOFMS has been described in detail elsewhere (*48*, *49*). The UF-ATOFMS has a high-particle transmission efficiency and measures the aerodynamic size and the positive and negative ion mass spectra of single particles in the size range between 50 and 300 nm. The last column in Table S1 shows the total number of particles that were chemically analyzed by the UF-ATOFMS for each vehicle and cycle.

The federal test procedure (FTP) and the unified cycle (UC) are both transient cycles, with the UC cycle having faster accelerations and higher speeds than the FTP cycle. Both cycles have a 10-min soak period where the engine is turned off before completing the cycle. The correction cycle (CC) is mostly a high-speed cruise. See the Supplemental Information section for the time-speed trace of each cycle as well as a more detailed description of each cycle. For the five TWC light-duty trucks (LDTs), the FTP and UC cycles were only run up until the 10-min soak period. These shorter FTP and UC cycles are referred to as FTPb12 and UCb12. With the exception of the TWC LDTs, all vehicles were run "cold", while the TWC LDTs were run "hot". Hot means that the vehicle was prepped by driving the vehicle at 50 mph for 10 min before being run through the testing cycle. Cold means that the vehicle was prepped and then kept in a temperature-controlled room for at least 12 h prior to testing and then pushed onto the dynamometer immediately prior to testing.

Results and Discussion

Scaling. The same procedures used for scaling ATOFMS counts with an optical particle counter described by Allen et al. and Wenzel et al. were applied in this study, except an SMPS was used as the reference instrument (*50*, *51*). See the Supplemental Information section for a description of the steps taken to ensure quality assurance of the UF-ATOFMS data as well as for a detailed explanation of the scaling procedure. Raw UF-ATOFMS counts were scaled to the SMPS for all particles with sizes between 50 and 180 nm. No corrections were made to the SMPS mobility diameters prior to scaling the UF-ATOFMS aerodynamic diameters since proper correction requires knowledge of many factors including particle density and shape (*52*−*54*). It has been shown that because of the particle fractal geometries, the mobility diameters of diesel soot particles can be larger than their aerodynamic diameters. Van Gulijk et al. found the following relationship between mobility (D_m) and aerodynamic diameters (D_a) (*52*):

$$\log(D_a) = 0.5012 \log(D_m) + 0.8267$$

To test how much this conversion affects the scaled results presented herein, the aerodynamic diameters of the ultrafine EC particles were converted to mobility diameters using the above equation. The diameters of the other particle types were not adjusted since these particle types do not have the same fractal geometries as EC. The percentages of EC particle types obtained with and without the diameter adjustment were compared. It was found that the ultrafine EC particle types were only overestimated by 7% without the diameter correction.

For scaling, the ratio of the unscaled UF-ATOFMS number concentration measured for a given size range divided by

the SMPS number concentration of particles in the same size range provides the particle detection efficiency for each size range. No modifications were made to adjust for chemical biases since it was determined these were negligible for this study over the size range studied (see Figures S6, S7, and S10 and relevant discussion in Supplemental Information). The inverse of this ratio gives the scaling factor needed to convert the unscaled ATOFMS number concentration into the true number concentration. The scaling factors were calculated for five size bins in the 50−180 nm range. An average scaling factor was calculated for each size bin for each vehicle, test, and cycle. All data presented in this paper have been scaled to take into account the transmission and detection efficiencies, as well as dilution conditions used for sampling. The data are reported as number emission factors (NEFs or number of particles emitted from the vehicle per gram of CO_2 emitted during the cycle).

In some instances, there were not enough UF-ATOFMS counts in a size bin to accurately scale the chemical information. A limit of 10 particles was chosen for the cutoff point, and the majority of the size bins had many more particles than this (Supplemental Information, Figure S9). To preserve the total number concentration and size profiles, the number concentrations of the nonscaled size bins were added as the "§" class and treated the same as the other classes. The chemically resolved UF-ATOFMS data were not scaled for the two smoker vehicles. The particle concentrations produced by these two vehicles were so high that the UF-ATOFMS experienced coincidence errors which made the size data unreliable (*55*). However, since the UF-ATOFMS utilizes a micro-orifice uniform deposit impactor (MOUDI) with the last stage removed as an upper size cut, the particles analyzed were predominately less than 300 nm. Thus, the chemical types of particles for the smoker vehicles will be discussed but not their absolute or relative number concentrations.

Chemical Classes. In this section, the compositions of the basic particle types observed are described. The analysis presented here discusses only those particles which produced both a positive and negative ion mass spectrum. A total of 16 026 particles were analyzed from all vehicles and tests. A significant fraction (43%) of particles measured during this study did not produce negative ions. Ambient studies by Bein et al. have shown similarly low percentages (22%) of negative ions, particularly for EC particles (*56*). There are several possibilities that would explain the lack of negative ions in these studies: (a) the mass spectrometer region of the UF-ATOFMS was not tuned properly (i.e., instrumental issues), (b) certain LDV particle types do not produce negative ions (i.e., chemical issues), or (c) a combination of both. If the reason for the lack of negative ions was due solely to instrumental issues, it would make sense to not include these particles in future source apportionment studies. However, if the lack of negative ions occurred because of chemical/source differences (i.e., the second case), this could be used as an additional piece of information in source apportionment studies. At this point, the reason for the lack of negative ions remains open until further source and lab studies are completed. In general, each polarity provides complimentary chemical information (*37*, *57*). For example, metal ions and organic fragment ions dominate the positive ion mass spectra, whereas nitrate, sulfate, silicate, metal oxides, and oxidized organic fragment ions dominate the negative ion mass spectra. No single chemical marker is unique to LDV emissions, but certain ion combinations with specific ratios will be used for apportionment purposes. Potential combinations are highlighted in the descriptions of the classes given below. The particle spectra were classified into general classes using a neural network (ART-2a) which groups particle mass spectra into clusters on the basis of similarities in their ion patterns. A vigilance factor of 0.85, a learning rate of 0.05, and 20 iterations were used (*58*, *59*). Digital mass spectra (*60*) for each resulting cluster were plotted to ensure that the particles were not improperly assigned to the incorrect class as well as to determine which clusters could be manually combined into one of 10 simplified classes. Clusters were manually combined into one class if they exhibited all of the following: similar mass spectra (e.g., the same exact combination of ion peaks with slightly varying intensities), similar size profiles, and similar temporal profiles. An 11th class (unknown) contains all particles that did not fit into any of the 10 classes. This class (initially 12% of the dataset) was reanalyzed using ART-2a at a lower vigilance factor and the resulting classes were combined, if appropriate, with the 10 other classes. It was found that most of the spectra in this class were miscalibrated with an ion peak shifted to the incorrect m/z value. After this analysis, the unknown class contained 1% of the total particles. Positive and negative ion average area matrices for the 10 classes are presented in Figure 1. Positive and negative ion digital mass spectra for the same 10 classes are presented in the Supplemental Information, Figure S2. Both representations of the mass spectra are useful in the analysis since they provide complementary information. The area matrices provide an indication of the relative intensity of each of the ion peaks in the single particle mass spectra for a given class. Digital mass spectra display the fraction of particles in each class that contains a peak above a threshold value (area > 50 arbitrary units). For example, as shown in Figure S2a, about 85% of all particles in Carbon Class 1 have a peak at m/z 27 with an area >50 units. For the class descriptions below, the percentage of a specific chemical species (i.e., nitrate, sulfate, etc.) for a given class is derived from the digital mass spectra. To obtain the mass concentration for a given chemical species, peak intensities must be calibrated either through comparison with MOUDI mass concentrations or by running particle standards in laboratory studies (*61*). The percentages of phosphate and sulfate are given as a range in cases where two species can occur at the same m/z ratio (−97). The peak at m/z −97 is considered sulfate unless there is also a major peak at $^{-79}(PO_3)$ in the same spectrum. For these particles, the values at $^{-79}(PO_3)$ and $^{-80}(SO_3)$ are the lower range for phosphate and sulfate, respectively, while $^{-97}(H_2OPO_3/HSO_4)$ is the upper value for both phosphate and sulfate. For each chemical class, a brief descriptive name is given for each class on the basis of several prevalent m/z peaks in the positive and negative ion mass spectra. These names are used to refer to the classes in the figures and discussions in later sections; however, the reader is directed to the following paragraphs for a comprehensive description of the chemical classes.

Carbon Class 1 (EC−Ca−PO_3). Peaks that correspond to elemental carbon (EC: m/z C_n, where $n = 1-12$), calcium (^{40}Ca), and phosphate ($^{-79}PO_3$) dominate the mass spectral intensities in this particle class. Sulfate and organic carbon (OC) were also associated with these particles. See Figure 1a for the ion peak assignments. Nearly 100% of the time, Ca and phosphate are present in the same particle spectra. Figure 2 shows the ion intensities for Ca and phosphate increase at the same rate as size increases. The intensities are plotted on *y*-axes with different magnitudes which show the ATOFMS is ∼4−5 times more sensitive to Ca than phosphate. This difference in sensitivity leads to a divergence of the intensity curves for sizes below 140 nm where Ca is detected in the particles, but phosphate is below the detection limit. Thus, the Ca and phosphate are most likely coming from the same source which in this case is the lubrication oil. Both are known additives in the oil. Ca is used as a detergent in the form of Ca sulfonate, phenate, salicylate, or carbonate and is used to neutralize acids and keep insoluble contaminants in

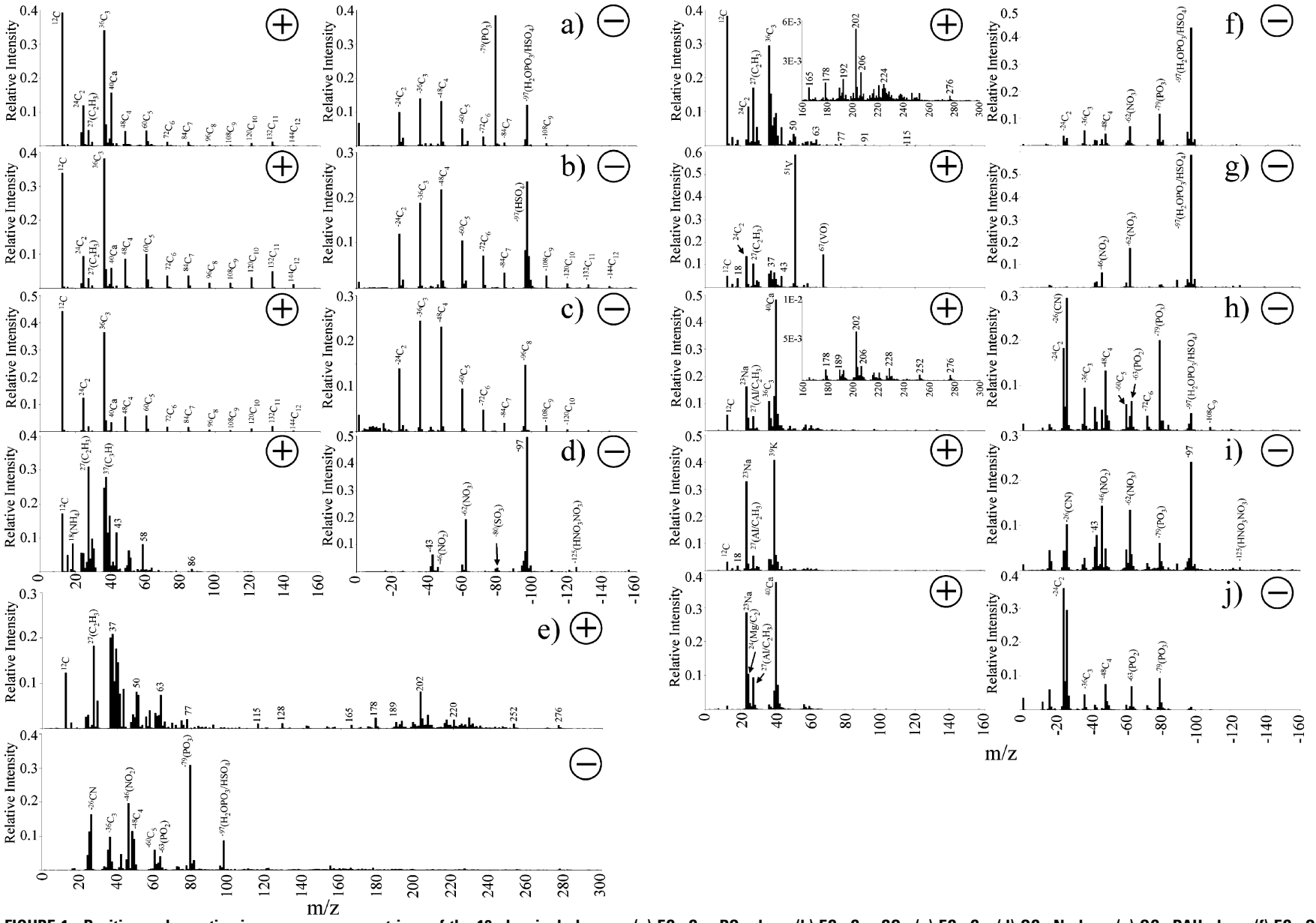

FIGURE 1. Positive and negative ion average area matrices of the 10 chemical classes: (a) EC−Ca−PO_3 class, (b) EC−Ca−SO_4, (c) EC−Ca, (d) OC−N class, (e) OC−PAH class, (f) EC−OC−aromatic class, (g) OC−V class, (h) Ca−EC−PO_3 class, (i) Na−K class, and (j) Na−Ca class.

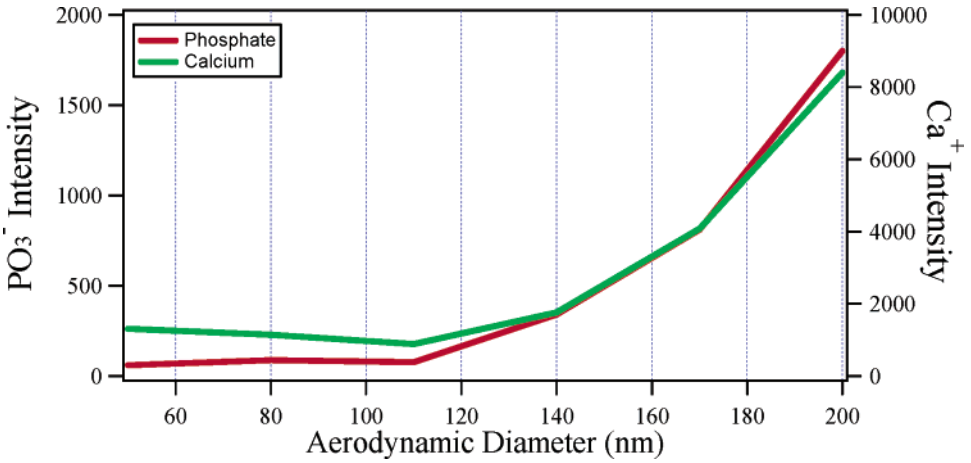

FIGURE 2. Mass spectral ion intensities for phosphate and Ca as a function of size for vehicles operating on the FTP cycle, showing a strong correlation between Ca and phosphate as size increases.

suspension. The phosphate is added in the form of zinc dialkyldithiophosphate as an antioxidant and antiwear additive (*62*, *63*). Thus, whenever Ca and phosphate appear in the same particle, it is highly likely that at least a portion of the particle originated from oil. EC (peaks at repeating C_n ion clusters) forms from the incomplete combustion of fuel and possibly oil. The OC fragments (*m*/*z* 27, 29, 39, 41, 43, 50, 51) are most likely from semivolatile species from the gasoline fuel or combustion byproducts (see Carbon Class 6 in Figure 1f). When EC particles are adsorbed in the oil, the dispersants (typically polyisobutylene amide succinimides) bind with the EC particles, keeping them from agglomerating together (*62*, *64*). The particles in this class most likely possess an EC core with OC on the surface (either the dispersants or combustion byproducts) which has been suggested by Sakurai et al. in previous vehicle studies (*65*). Previous roadside studies have proposed that the submicrometer Ca is being emitted from vehicles (gasoline and diesel) and the work herein supports those findings (*66*−*68*).

Carbon Class 2 (EC−Ca−SO_4). This class is very similar to Carbon Class 1 (EC−Ca−PO_3), except these particles contain no mass spectral peaks from phosphate and show more intense peaks because of sulfate (~100%), Figure 1b. The sulfate could be from the oil additive in the form of Ca sulfonate or the small fraction of sulfur in the gasoline fuel.

Carbon Class 3 (EC−Ca). This class is very similar to the first two carbon classes (EC−Ca−PO_3 and the EC−Ca−SO_4), except the particle mass spectra in this class contain only EC peaks in the negative ion spectra with at times small contributions from phosphate or sulfate, Figure 1c. These are typically the smallest particles detected with most occurring in the <100 nm size range (Figure 3). The Ca ion intensity in this class is the least intense of Carbon Classes 1−3. This is consistent with their smaller sizes as shown in Figure 2 where the ion intensity for Ca (and phosphate) decreases with particle diameter indicating less oil is associated with the smaller particles. ATOFMS has a higher sensitivity to metals than carbonaceous species (*69*), and thus the amount of Ca in all three of these particle types represents a small mass fraction of the total particle. The term "the three EC−Ca classes" will be used to collectively refer to Carbon Classes 1−3 in later sections, while the term "EC−Ca" refers to Carbon Class 3. It is possible that particle spectra in Carbon Classes 1−3 were just desorbed/ionized by different parts of the inhomogeneous laser beam producing different ion intensity patterns (*69*, *70*). However, they have different sizes, are produced during different cycles, and originate from different vehicles (see Figures 3−5), indicating that they are most likely of different origin. For

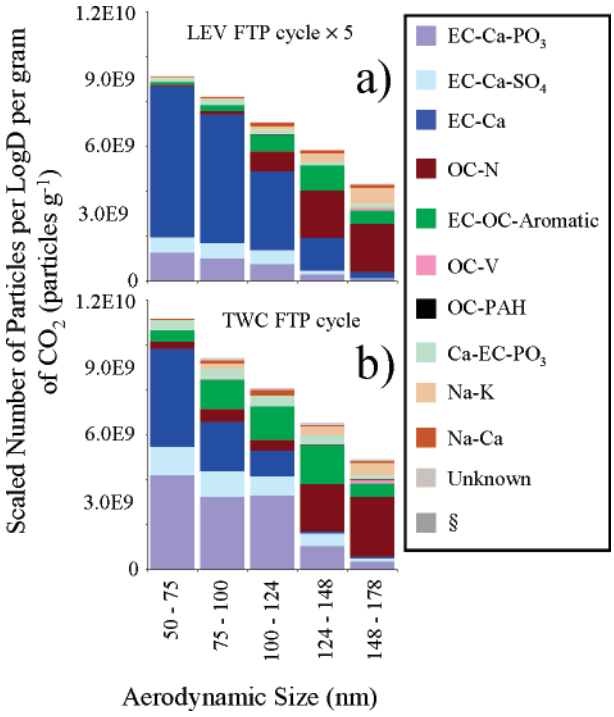

FIGURE 3. Representative size profiles of the 12 classes for the LEV and TWC vehicles on the FTP cycle in the 50−180 nm size range.

the purposes of this paper, given the distinctly different signatures in the negative ion mass spectra, these particles were kept in separate classes.

Carbon Class 4 (OC−N). This carbon class contains OC, sulfate (90%), and nitrate (82%) in addition to semivolatile species including ammonium (85%) and nitrogen-containing organic species such as amines, Figures 1d. Ammonia (which can react with nitric acid to form ammonium nitrate) can be formed in the three-way catalytic converter as a byproduct of the process which reduces NO_x to N_2 under rich fuel−air mixture conditions (*71*). This class is detected in particles sampled from all vehicles equipped with three-way catalytic converters. Markers used to identify amines occur at $^{58}(C_3H_5N)$ and $^{86}(C_5H_{12}N)$ (*32*). Other OC signatures (*m*/*z* 27, 29, 43, and 50) in the mass spectra indicate the presence of unburned or partially burned gasoline fuel. The lack of Ca and phosphate eliminates oil as the source of this particle type since an ATOFMS study on particles generated by aerosolizing a range of new and used oil and gasoline samples shows that the combination of Ca and phosphate is always

TABLE 1. List of Possible PAHs for Each *m/z* Ratio

m/z	PAH
128	naphthalene
152	acenaphthylene
178	anthracene
192	methyl anthracene
192	methyl phenanthrene
202	pyrene
202	fluoranthene
206	dimethyl phenanthrene
216	methyl pyrene
220	trimethyl anthracene
220	trimethyl phenanthrene
228	chrysene
228	benzo[a]anthracene
252	benzo[a]pyrene
252	benzo[b]fluoranthene
276	benzo[ghi]perylene
276	indeno[123cd]pyrene

present in particles produced from oil while being absent in gasoline particles (*57*).

Carbon Class 5 (OC−PAH). Particle spectra in this carbon class show the presence of PAHs, along with phosphate, OC, and EC (Figure 1e). PAHs were detected at *m/z* 128, 152, 178, 192, 202, 206, 216, 220, 228, 252, and 276. Because of the high laser fluence used in this study, fragmentation occurred for most organic compounds, however, PAHs have been shown to also yield parent ions even under these laser power conditions (*29*). Fragments of the PAHs or monoaromatics are seen at *m/z* 50, 51, 63, 77, 91, 115, 165, and 189 (*29*, *72*). Table 1 shows some possible PAHs that could account for each of these ion peaks that have been identified in previous LDV dynamometer studies (*11*, *13*, *15*, *73*) and, except for the methyl-substituted PAHs, identified in liquid gasoline samples (*74*). The methyl-substituted PAHs listed in Table 1 were detected in used gasoline oil (*75*). The PAHs detected in this study have also been identified in tunnel and roadside studies (*66*, *76*−*79*).

Carbon Class 6 (EC−OC−Aromatic). The particle spectra in this class have peaks indicative of EC (m/z ^{12}C, $^{24}C_2$, $^{36}C_3$, $^{-24}C_2$, $^{-36}C_3$, and $^{-48}C_4$) and OC. The particle spectra for this type also contained sulfate (20−75%) and phosphate (50−75%), Figure 1f. In addition to substituted monoaromatic compounds, peaks at *m/z* 15, 27, 29, 41, and 43 most likely represent alkyl fragments from organic compounds in the fuel and oil. This class also contains a small percentage (6%) of PAHs. This class is most likely unburned gasoline fuel or combustion byproducts condensed onto an insoluble core, such as the EC species observed in the same spectra. Aromatic species have been shown to represent a significant fraction of the volatile and semivolatile species in gasoline and have been shown to lead to secondary organic aerosol production in the atmosphere (*80*).

Carbon Class 7 (OC−V). This class of carbon particle spectra contains strong signals from vanadium and vanadium oxide, in addition to OC, sulfate (50−95%), nitrate (95%), ammonium (90%), and phosphate (45−95%), Figure 1g. Vanadium is naturally present in petroleum and has been associated with the combustion of petroleum (*81*, *82*). It should have low concentrations in the exhaust and is not expected to be a dominant class. This class represented only 1% of the total particle counts but it is highlighted because of potential health effect issues (*83*). It was detected in nearly all of the vehicles tested, and thus, is a possible candidate for a vehicle marker ion in source apportionment studies when used in conjunction with other ion markers in the same spectra. This particle type has been identified in previous ambient single particle mass spectrometry studies, although usually in low abundance (*84*, *85*).

Inorganic Class 1 (Ca−EC−PO_3). This class is a mixture of OC and EC with phosphate, sulfate, and nitrate mixed with several different metals, Figure 1h. The metals include Ca, Na, Mg, Al, and K. A small percentage (20%) of the particles in this class also contained the same PAH species observed in the OC−PAH class. The signature for this class differs from the EC−Ca classes with the Ca peak being more intense than the rest of the EC peaks in the mass spectrum. In addition, the three EC−Ca classes peak in the ultrafine mode (D_a < 100 nm) while the Ca−EC−PO_3 class peaks in the fine mode (100 < D_a < 300 nm).

Inorganic Class 2 (Na−K). Mass spectra in this class contain Na, K, Ca, Mg, and Al along with EC (60%), OC (60%), phosphate (50−70%), sulfate (55−70%), and nitrate (75%) (Figure 1i). This class is detected in the nebulization of gasoline fuel (*57*) and likely results from incomplete combustion of gasoline fuel. These same inorganic species have been detected in previous light-duty vehicle dynamometer studies (*12*, *14*, *73*).

Inorganic Class 3 (Na−Ca). This class contains primarily metals (Na, K, Ca, Mg, and Al) with EC (70%), OC (30%), phosphate (25−50%), and sulfate (25−30%) (Figure 1j). One likely source of this class is oil additives. Antiwear additives in the oil polymerize, forming 20−100 nm thick films consisting of iron or the overbase metal (Ca or Mg), phosphorus, sulfur, and oxygen as well as some organic material (*62*). These films can be mechanically broken up and emitted through the exhaust system as particles. This class could also originate from the combustion of the gasoline fuel. In general, all particles in the inorganic classes detected during this study show similarities to atmospheric dust and soil particles. In fact, particles with similar signatures to this class have been detected near an autobahn using single particle mass spectrometry and named "mineral and carbonaceous" and attributed to soil dust (*68*). The major feature which distinguishes inorganic vehicle particle types from atmospheric dust particles is a lack of silicates in the vehicle particles.

Size. Figure 3 shows the average scaled ATOFMS number emission factor (NEF) of the 12 classes in the 50−180 nm size range for the LEV (Figure 3a) and TWC (Figure 3b) vehicles. Analogous plots for all of the individual car categories are shown in the Supplemental Information (Figure S3). The size range between 180 and 300 nm is not shown because of very low particle counts detected. The UF-ATOFMS samples from the last stage of a MOUDI, which has a 50% size cut at 100 nm to remove the majority of particles larger than 250 nm (*48*). Filter measurements confirm that the majority of the mass occurred below 180 nm (*47*).

In the 50−100 nm size range, close to 85% of the particles are dominated by EC signatures. OC begins to make larger contributions for particles with sizes larger than 100 nm as described below. Several previous LDV dynamometer studies have measured mostly OC particles and very little EC (*11*, *12*, *14*), while other studies show variations ranging between 2 and 38% in the EC to total carbon ratio (*13*, *15*, *86*). All previous dynamometer studies measure PM mass fractions, whereas in this study the reported percentages are based on PM numbers. However, simultaneous filter measurements made by the Kleeman group show the EC/OC mass ratio of 0.6 for the average of all tests for ultrafine particles with LEVs showing a EC/OC ratio of 2.52 (*47*). To convert number concentrations to mass concentrations, the aerodynamic diameters must be converted to physical diameters using the effective density and shape factors. The EC−Ca classes also had OC associated with them (i.e., 70−85% of the particles in these classes have a detectable OC peak, m/z $^{27}(C_2H_3)$). The relative fraction of OC on the EC particles increases as a function of size as shown in Figure 4 which shows the OC/EC ion intensity ratios for all particles sampled

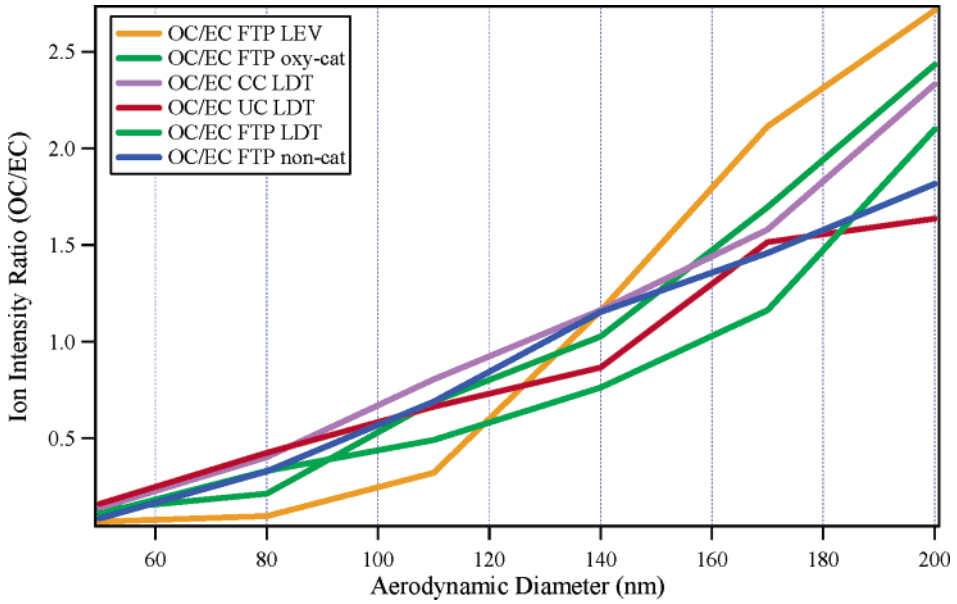

FIGURE 4. Ratio of ion intensities for OC/EC as a function of size for all particles sampled from different vehicle and cycle categories, showing an increase as a function of size.

as a function of size for several vehicle-cycle combinations. This plot is based on all particles and thus provides more of a bulk perspective. The observed size-resolved OC/EC ratios were comparable to those observed for particles in this same size range in ambient studies. A future publication will present results on the quantitatition of OC on EC particles using the measured ATOFMS intensity ratios in the mass spectral data (*87*). Quantifying the relative amount of EC versus OC is challenging as evidenced by the wide range of values reported in the literature. The main method used for EC/OC quantification is sensitive to the temperature program (*88*, *89*). All of these issues (the EC/OC split, mass versus number, the density of EC versus OC, the ATOFMS sensitivity to EC and OC) need to be taken into account when comparing the results presented herein with those from previous dynamometer studies.

In the 100−180 nm size range, the EC−OC−aromatic and the OC−N classes are more abundant than in the smaller sizes, while the EC dominated classes become less abundant. This is expected because the EC−OC−aromatic and the OC−N particles most likely form as EC particles become more coated with semivolatile OC species. As particles become coated with OC, the EC ion intensities become suppressed, as observed in previous ^{13}C particle coating experiments in our laboratory (*90*). The results for this size range agree with other dynamometer studies which show mostly OC above 100 nm (*11*−*15*).

Vehicle and Cycle Variability. Figure 5 displays the scaled ATOFMS NEFs for particles in the size range between 50 and 180 nm for each of the five TWC light-duty trucks (LDTs) on three cycles. The "§" class is large for the Dodge Caravan because of low UF-ATOFMS counts in the smallest size bins. The reader is referred back to the Scaling section for a more complete explanation of the "§" class. The ATOFMS mass spectra showed the Dodge Caravan emitted high amounts of larger sized Ca and phosphate particles more closely resembling those emitted from the smoking vehicles than the other vehicles in the same category (TWC LDTs), suggesting it may have fit more appropriately in the smoker category. Significant variation was observed in the total NEFs and chemical composition within the TWC LDT category. In fact, there were large variations between vehicles in all of the car categories. See the Supplemental Information (Figure S4) for the other car category plots that are analogous to Figure 5. For most of the LDT vehicles and cycles, the three EC−Ca classes were dominant. For the Suzuki Samari and Chevrolet Suburban, larger sized particles in the EC−OC−aromatic and OC−PAH classes made higher contributions to the total NEFs.

Four of the five vehicles produced higher NEFs on the UCb12 cycles (shorter UC cycle) than the CC cycle or the shorter FTP (FTPb12) cycle. As described in the Experimental Section, both the UC and the FTP cycles are transient cycles, with the UC cycle having significantly faster accelerations/decelerations and higher speeds. The CC cycle is mostly a high-speed cruise cycle. See the Supplemental Information for the time-speed trace for all of the cycles. Overall, the five light-duty trucks produced more particles under faster accelerations and at higher speeds. This increase was also seen for the six TWC passenger cars, which were tested on the FTP and UC cycles (Supplemental Information, Figure S4). In general for unscaled ATOFMS counts, a higher relative fraction of OC to EC particle types were observed on the FTP cycle than the UC cycles. In general, for all the passenger cars, the positive ion signatures remained almost identical with most of the composition change occurring in the negative ions. Comparing the FTP to the UC cycle for the same passenger cars, the negative ion spectra go from having nitrate and sulfate to mostly EC markers at m/z −24, −36, and −48, showing that more EC particles are produced overall under faster acceleration and higher speed conditions.

Particles per Mile Comparison with Literature. As a reminder, the goal of this study was to examine the PM emissions from a wide range of LDVs to derive appropriate signatures for ambient apportionment. However, for comparison purposes between studies, the data are reported in units of particles per gram of CO_2 so that one can estimate the total amount of pollution using actual fuel inventories. However, most of the literature reports NEFs with units of particles mile^{-1} driven. For comparison purposes, our data are converted into particles mile^{-1}. The measured NEFs values range from 3×10^{11} to 10^{15} particles mile^{-1}, with the majority of the reported values in the 10^{13}−10^{15} range (*91*−*95*). All of the vehicles fall within this range, with the LEVs having the lowest NEFs (an average of 3×10^{11} particles mile^{-1}, ranging from 1.0×10^{10} to 9.6×10^{11} particles mile^{-1}). The non-LEVs in this study have NEFs that range from 5.6×10^{10} to 1.5×10^{14} particles mile^{-1}, with the newer technology vehicles

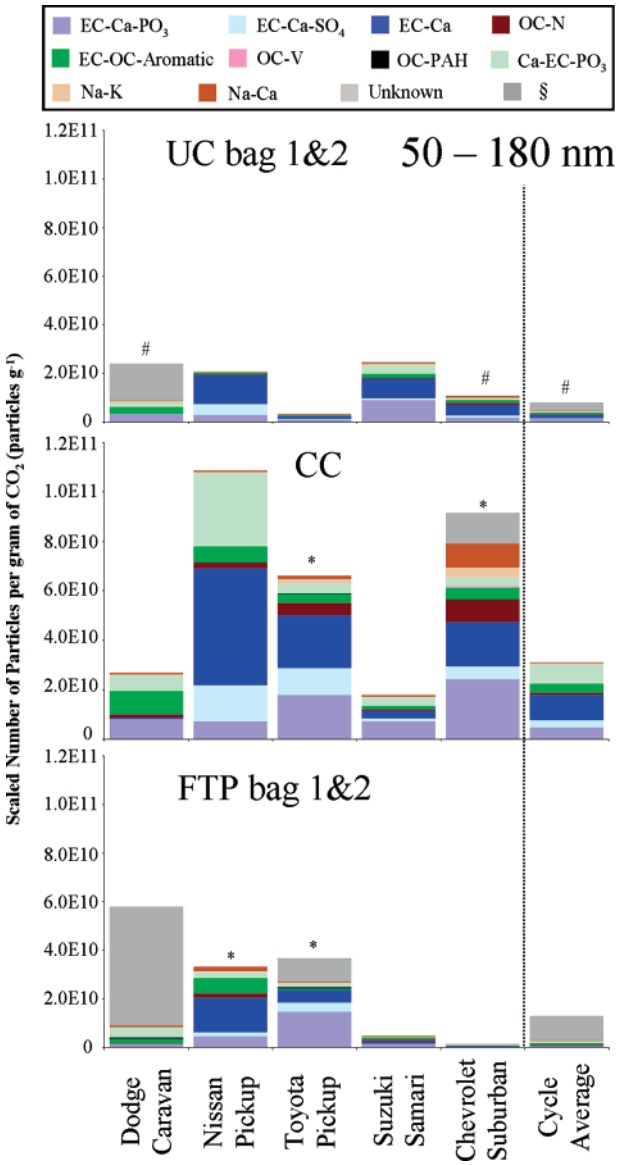

FIGURE 5. Scaled number concentrations (NEF values) of the 12 classes for the TWC light-duty trucks on three different cycles. Note the counts for bars with an (*) were multiplied by 100 and the bars with a (#) were divided by 10 to be visible on the same *y*-axis scale.

having the lower NEFs and the smoker vehicles having the highest NEFs. The observation that the oxidation catalysts, noncatalysts, and smoker vehicles have higher NEFs than the LEVs and TWCs is expected on the basis of their older engine technologies.

Cold Start. While it has been documented that cold starts produce the majority of the emissions (*96*−*98*), few results have been presented regarding the chemical composition of the particle types emitted during the early stages of the FTP cycle because of difficulties associated with obtaining enough material for chemical analysis in such a short time period. Recent studies have made high temporal resolution measurements of size-resolved chemistry of the refractory materials in vehicular PM emissions; however, they were unable to probe the temporal evolution of EC particles (*27*, *65*). To investigate composition changes occurring with 2-min resolution, the UF-ATOFMS counts for all 10 LEV vehicles tested on the FTP cycle with a cold start were combined. Figure 6 shows chemical changes occurring with 2-min resolution of the scaled UF-ATOFMS NEFs for 50−180 nm particles. The CO_2 data (originally in grams of CO_2 per mile

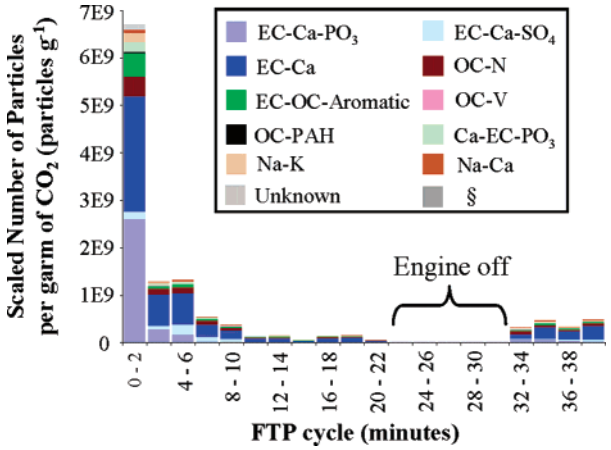

FIGURE 6. Two-minute temporal profile of the 12 classes for the 10 LEV vehicles on the FTP cycle for all particles between 50 and 180 nm size range. A cooling period, indicated by a gap when the vehicle engine was off, occurred from 22 to 32 min and then the cars were restarted at 32 min.

driven) were only available in three segments (taken in bags) of the FTP cycle (bag 1 (first 505 s), bag 2 (506−1374 s), and bag 3 (last 505 s)). The NEFs were calculated using the miles driven during each 2-min segment with the corresponding average bag value of grams of CO_2 per mile driven. The NEF decreases as the engine temperature increases (a factor of 5 from 2 to 6 min after the cycle begins and a factor of 50 after 10 minutes). Ultrafine EC−Ca−PO_3 and the EC−Ca classes dominate the PM emissions during the cold start and exist for the first 3−5 min of the cycle. The absolute (and relative) NEFs of the EC−Ca−PO_3 class decrease as the engine warms (a factor of 9 after 2 min and more than a factor of 75 after 6 min).

The first 505 s of the FTP cycle were repeated after a 10-min soak (the hot engine is turned off), and the NEFs measured for the hot start (first 2 min) do not reach the same levels as the cold start (a factor of 20 lower). In the hot start, the dominant classes are again the EC−Ca−PO_3 and the EC−Ca classes. The NEF of the EC−Ca−PO_3 class decreased to 65% of its cold start value by the end of the FTP cycle. No other chemical class had such a large decrease in the NEF value (the OC−N and the EC−OC−aromatic classes remained relatively constant over the full cycle only decreasing by 12% and 15%, respectively). In summary, compared to the other chemical classes, the EC−Ca−PO_3 class is preferentially produced during starts (cold and hot); however, the most obvious change was in the total absolute number concentration as previously reported.

Exhaust Technology. Figure 7 shows the NEFs for each of the car categories tested on the FTP cycle for particles in the 50−180 nm size range. Each bar represents the average NEF for all vehicles in each category. This figure shows that regardless of the engine technology, the same major particle types are present for all vehicles, but the absolute number concentrations vary. The general composition differences are most apparent when comparing different fractions of EC and OC particle types as a function of size. With the exception of the smoker category (2.4×10^{11} particles per gram of CO_2), the general trend is that older engine technologies (noncat, oxy-cat) produced the most and that newer technologies (LEV, TWC: 7.9×10^8 particles gram of CO_2 and 4.7×10^9 particles gram of CO_2, respectively) produced the least particles. This is consistent with the work by Bishop and Stedman who report that 10% of the vehicle fleet emit over 50% of the gas-phase emissions (*99*). Given that the majority of those high-emitting vehicles had defective emission control systems (*99*), it is also likely that they emitted high levels of

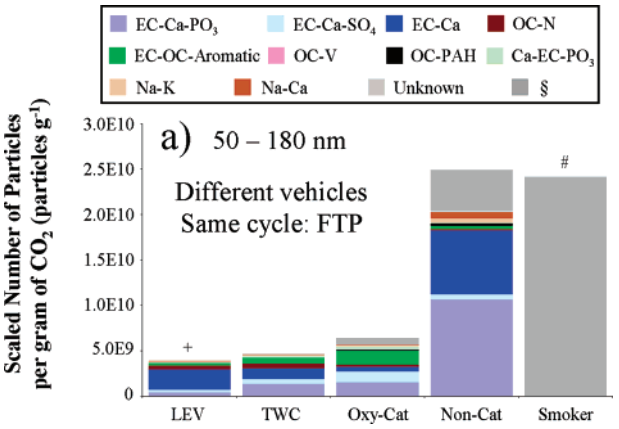

FIGURE 7. NEFs of the 12 classes for each of the car categories tested on the FTP cycle for particles in the 50−180 nm size range. The bar with a (+) indicates multiplication by 5 and the bar with a (#) indicates division by 10. For the oxy-cat cycle, one vehicle (#23 shown in S4 and S5) was removed because of instrumental issues.

PM as well. The vehicles equipped with three-way catalytic converters (LEV and TWC) produced relatively more particles in the OC−N class than the rest of the vehicle categories. As discussed in the Chemical Classes section, this particle type contained ammonium, which is a byproduct of the reduction of NO_x to N_2 under rich fuel−air mixture conditions in three-way catalytic converters (*71*).

Seagrave et al. found that PM and semivolatile organic compounds (SVOCs) from high PM mass emitting (smoker) vehicles have higher toxicity per unit mass than normal emitting vehicles (*100*). This is most likely at least partly because the higher fraction of aromatic and PAHs as well as used oil are produced by smoker vehicles, as reported in this work as well as by others (*13*, *15*, *73*). A substantial fraction (76%) of the particles emitted by the smokers showed associations with Ca and phosphate, indicating used lubrication oil was being emitted by the smoker vehicles. This finding is consistent with the cars in this class being labeled as "blue" smokers which are known to release oil. The oxy-catalyst category also showed high fractions of particles with Ca and phosphate signatures. In general, more Ca and phosphate (both number and mass spectral intensity) indicate more oil emitted, corresponding with more OC detected on the filters (*47*). Because the smoker category could not be scaled because of the extremely high number of particles produced, the calculated percentage is based on raw particle counts. Over the measured size range, 26% of the particles produced by the smoker category vehicles belonged to the EC−OC−aromatic and OC−PAH classes, which is ~6 times higher than the average for the rest of the car categories.

An interesting finding from this study is how more (and larger) particles containing oil are emitted during fast accelerations (i.e., UC cycle) and cold starts, as well as from smokers and vehicles with older engine technologies (i.e., oxy-catalyst). These particles typically have larger sizes and thus make significant contributions to particle mass measurements of OC (i.e., $PM_{2.5}$). It has been well documented that unburned oil is one of the major species being emitted from HDV as well (*43*, *45*, *65*). This could make differentiating LDV from HDV quite challenging when an apportionment study is performed in areas where there are a higher number of older or more poorly maintained vehicles or near a roadway where fast accelerations occur.

The OC−PAH class was the only chemical class in which $^{-46}(NO_2)$ was present in more particles than $^{-62}(NO_3)$. Nitrate-containing particles, when analyzed using ATOFMS, yield peaks at $^{-62}(NO_3)$ and $^{-46}(NO_2)$ and usually, the $^{-46}(NO_2)$ peak shows a lower abundance than $^{-62}(NO_3)$. Since the OC−PAH class showed the reverse trend, this may be an indication of other species, such as nitro-PAHs, contributing to $^{-46}(NO_2)$. In previous laser desorption/ionization studies of nitro-PAH, these species have been shown to rapidly fragment to produce an intense peak at $^{-46}(NO_2)$ (101). Nitro-PAHs are highly carcinogenic and mutagenic (*102*, *103*) and have been previously detected in vehicle exhaust (*104*, *105*). Therefore, reducing the number of high PM emitters on the road would not only have a dramatic effect in lowering the amount of PM and SVOCs released into the environment from vehicle traffic but could also result in a reduction in the amount of mutagenic and carcinogenic compounds released as well.

Acknowledgments

The authors would like to sincerely thank Shane Michael and the rest of the crew at the Haggen-Smit Laboratory in El Monte for driving the vehicles and for their hard work and dedication to this project as well as William Vance from the California Air Resources Board (CARB) for the detailed vehicle information and valuable scientific discussions. We also sincerely thank Michael Kleeman, Michael Robert, and Chris Jakober for operating the dilution and residence chamber. Funding for this project was supplied by the CARB.

Supporting Information Available

Table S1 displays the make, model, year, mileage, and cycles driven for each vehicle as well as the total number of chemically analyzed particles by the UF-ATOFMS (50−180 nm). Figure S1 shows the time-speed traces for each of the cycles driven, FTP, UC, and UCC50. Figure S2 provides the positive and negative ion digital mass spectra for the 10 chemical classes. Figure S3 shows the NEFs size-resolved chemical information for the individual car categories. Figure S4 shows the scaled NEFs for each vehicle in the 50−180 nm size range. Figure S5 shows the normalized scaled NEFs for each vehicle where the relative contributions of each class for each vehicle are more readily visible. A discussion of the quality assurance steps taken as part of the data analysis process is presented, as well as a detailed discussion of the steps taken during the scaling procedure. Figure S6 displays the hit fraction as a function of size for each vehicle-cycle combination. Figure S7 shows the hit fraction as a function of time and size for all LEVs on the FTP cycle. Figure S8 shows a flow diagram of the scaling procedure. Figure S9 shows the ATOFMS counts per size bin for all vehicle-cycle combinations. Figure S10 shows the range of scaling functions used to scale ATOFMS number concentrations to true number concentrations. This material is available free of charge via the Internet at http://pubs.acs.org.

Literature Cited

(1) Vanvorst, W. D.; George, S. Impact of the California Clean Air Act. *Int. J. Hydrogen Energy* **1997**, *22*, 31−38.
(2) Mysliwiec, M. J.; Kleeman, M. J. Source apportionment of secondary airborne particulate matter in a polluted atmosphere. *Environ. Sci. Technol.* **2002**, *36*, 5376−5384.
(3) Marshall, J. D.; Riley, W. J.; McKone, T. E.; Nazaroff, W. W. Intake fraction of primary pollutants: Motor vehicle emissions in the South Coast Air Basin. *Atmos. Environ.* **2003**, *37*, 3455−3468.
(4) Fruin, S. A.; St Denis, M. J.; Winer, A. M.; Colome, S. D.; Lurmann, F. W. Reductions in human benzene exposure in the California South Coast Air Basin. *Atmos. Environ.* **2001**, *35*, 1069−1077.
(5) Fenn, M. E.; Haeuber, R.; Tonnesen, G. S.; Baron, J. S.; Grossman-Clarke, S.; Hope, D.; Jaffe, D. A.; Copeland, S.; Geiser, L.; Rueth, H. M.; Sickman, J. O. Nitrogen emissions, deposition, and monitoring in the western United States. *Bioscience* **2003**, *53*, 391−403.
(6) Ying, Q.; Mysliwiec, M.; Kleeman, M. J. Source apportionment of visibility impairment using a three-dimensional source-oriented air quality model. *Environ. Sci. Technol.* **2004**, *38*, 1089−1101.

(7) Laden, F.; Neas, L. M.; Dockery, D. W.; Schwartz, J. Association of fine particulate matter from different sources with daily mortality in six US cities. *Environ. Health Perspect.* **2000**, *108*, 941−947.
(8) Pope, C. A.; Burnett, R. T.; Thun, M. J.; Calle, E. E.; Krewski, D.; Ito, K.; Thurston, G. D. Lung cancer, cardiopulmonary mortality, and long-term exposure to fine particulate air pollution. *J. Am. Med. Assoc.* **2002**, *287*, 1132−1141.
(9) Clancy, L.; Goodman, P.; Sinclair, H.; Dockery, D. W. Effect of air-pollution control on death rates in Dublin, Ireland: An intervention study. *Lancet* **2002**, *360*, 1210−1214.
(10) Strauss, K. H.; Dukek, W. G. *The impact of U.S. environmental regulations on fuel quality*; ASTM: Philadelphia, PA, 1993.
(11) Schauer, J. J.; Kleeman, M. J.; Cass, G. R.; Simoneit, B. R. T. Measurement of emissions from air pollution sources 5: C-1-C-32 organic compounds from gasoline-powered motor vehicles. *Environ. Sci. Technol.* **2002**, *36*, 1169−1180.
(12) Kleeman, M. J.; Schauer, J. J.; Cass, G. R. Size and composition distribution of fine particulate matter emitted from motor vehicles. *Environ. Sci. Technol.* **2000**, *34*, 1132−1142.
(13) Cadle, S. H.; Mulawa, P. A.; Hunsanger, E. C.; Nelson, K.; Ragazzi, R. A.; Barrett, R.; Gallagher, G. L.; Lawson, D. R.; Knapp, K. T.; Snow, R. Composition of light-duty motor vehicle exhaust particulate matter in the Denver, Colorado area. *Environ. Sci. Technol.* **1999**, *33*, 2328−2339.
(14) Cadle, S. H.; Mulawa, P. A.; Ball, J.; Donase, C.; Weibel, A.; Sagebiel, J. C.; Knapp, K. T.; Snow, R. Particulate emission rates from in use high emitting vehicles recruited in Orange County, California. *Environ. Sci. Technol.* **1997**, *31*, 3405−3412.
(15) Sagebiel, J. C.; Zielinska, B.; Walsh, P. A.; Chow, J. C.; Cadle, S. H.; Mulawa, P. A.; Knapp, K. T.; Zweidinger, R. B. PM_{10} exhaust samples collected during IM-240 dynamometer tests of in-service vehicles in Nevada. *Environ. Sci. Technol.* **1997**, *31*, 75−83.
(16) Chow, J. C.; Watson, J. G.; Kuhns, H.; Etyemezian, V.; Lowenthal, D. H.; Crow, D.; Kohl, S. D.; Engelbrecht, J. P.; Green, M. C. Source profiles for industrial, mobile, and area sources in the Big Bend Regional Aerosol Visibility and Observational study. *Chemosphere* **2004**, *54*, 185−208.
(17) Watson, J. G. Visibility: Science and regulation. *J. Air Waste Manage. Assoc.* **2002**, *52*, 628−713.
(18) Hopke, P. K. Recent developments in receptor modeling. *J. Chemom.* **2003**, *17*, 255−265.
(19) Kim, E.; Larson, T. V.; Hopke, P. K.; Slaughter, C.; Sheppard, L. E.; Claiborn, C. Source identification of PM2.5 in an arid Northwest US City by positive matrix factorization. *Atmos. Res.* **2003**, *66*, 291−305.
(20) Schauer, J. J.; Rogge, W. F.; Hildemann, L. M.; Mazurek, M. A.; Cass, G. R. Source apportionment of airborne particulate matter using organic compounds as tracers. *Atmos. Environ.* **1996**, *30*, 3837−3855.
(21) Schauer, J. J. Evaluation of elemental carbon as a marker for diesel particulate matter. *J. Exp. Anal. Environ. Epidemiol.* **2003**, *13*, 443−453.
(22) Zhang, Q.; Canagaratna, M. R.; Jayne, J. T.; Worsnop, D. R.; Jimenez, J. L. Time- and size-resolved chemical composition of submicron particles in Pittsburgh: Implications for aerosol sources and processes. *J. Geophys. Res., Atmos.* **2005**, *110*, DO7S09; doi: 10.1029/2004JD004649.
(23) Glagolenko, S.; Phares, D. J. Single-particle analysis of ultrafine aerosol in College Station, Texas. *J. Geophys. Res., Atmos.* **2004**, *109*, D18205; doi: 10.1029/2004JD004621.
(24) Hudson, P. K.; Murphy, D. M.; Cziczo, D. J.; Thomson, D. S.; de Gouw, J. A.; Warneke, C.; Holloway, J.; Jost, J. R.; Hubler, G. Biomass-burning particle measurements: Characteristic composition and chemical processing. *J. Geophys. Res., Atmos.* **2004**, *109*, D23527; doi: 10.1029/2003JD004198.
(25) Guazzotti, S. A.; Suess, D. T.; Coffee, K. R.; Quinn, P. K.; Bates, T. S.; Wisthaler, A.; Hansel, A.; Ball, W. P.; Dickerson, R. R.; Neususs, C.; Crutzen, P. J.; Prather, K. A. Characterization of carbonaceous aerosols outflow from India and Arabia: Biomass/biofuel burning and fossil fuel combustion. *J. Geophys. Res., Atmos.* **2003**, *108* (D15), 4485; doi: 10.1029/2002JD003277.
(26) Sipin, M. F.; Guazzotti, S. A.; Prather, K. A. Recent advances and some remaining challenges in analytical chemistry of the atmosphere. *Anal. Chem.* **2003**, *75*, 2929−2940.
(27) Canagaratna, M. R.; Jayne, J. T.; Ghertner, D. A.; Herndon, S.; Shi, Q.; Jimenez, J. L.; Silva, P. J.; Williams, P.; Lanni, T.; Drewnick, F.; Demerjian, K. L.; Kolb, C. E.; Worsnop, D. R. Chase studies of particulate emissions from in-use New York City vehicles. *Aerosol Sci. Technol.* **2004**, *38*, 555−573.
(28) Morrical, B. D.; Fergenson, D. P.; Prather, K. A. Coupling two-step laser desorption/ionization with aerosol time-of-flight mass spectrometry for the analysis of individual organic particles. *J. Am. Soc. Mass. Spectrom.* **1998**, *9*, 1068−1073.
(29) Silva, P. J.; Prather, K. A. Interpretation of mass spectra from organic compounds in aerosol time-of-flight mass spectrometry. *Anal. Chem.* **2000**, *72*, 3553−3562.
(30) Zelenyuk, A.; Cabalo, J.; Baer, T.; Miller, R. E. Mass spectrometry of liquid aniline aerosol particles by IR/UV laser irradiation. *Anal. Chem.* **1999**, *71*, 1802−1808.
(31) Whiteaker, J. R.; Prather, K. A. Hydroxymethanesulfonate as a tracer for fog processing of individual aerosol particles. *Atmos. Environ.* **2003**, *37*, 1033−1043.
(32) Angelino, S.; Suess, D. T.; Prather, K. A. Formation of aerosol particles from reactions of secondary and tertiary alkylamines: Characterization by aerosol time-of-flight mass spectrometry. *Environ. Sci. Technol.* **2001**, *35*, 3130−3138.
(33) Hauler, T. E.; Boesl, U.; Kaesdorf, S.; Zimmermann, R. Mobile resonance enhanced multiphoton ionisation-time-of-flight mass spectrometer with a novel hybrid laser desorption/molecular beam ion source for rapid detection of aromatic trace compounds from gas phase and solid samples. *J. Chromatogr. A* **2004**, *1058*, 39−49.
(34) LaFranchi, B. W.; Zahardis, J.; Petrucci, G. A. Photoelectron resonance capture ionization mass spectrometry: a soft ionization source for mass spectrometry of particle-phase organic compounds. *Rapid Commun. Mass Spectrom.* **2004**, *18*, 2517−2521.
(35) Oktem, B.; Tolocka, M. P.; Johnston, M. V. On-line analysis of organic components in fine and ultrafine particles by photoionization aerosol mass spectrometry. *Anal. Chem.* **2004**, *76*, 253−261.
(36) Woods, E.; Smith, G. D.; Dessiaterik, Y.; Baer, T.; Miller, R. E. Quantitative detection of aromatic compounds in single aerosol particle mass spectrometry. *Anal. Chem.* **2001**, *73*, 2317−2322.
(37) Bhave, P. V.; Fergenson, D. P.; Prather, K. A.; Cass, G. R. Source apportionment of fine particulate matter by clustering single-particle data: Tests of receptor model accuracy. *Environ. Sci. Technol.* **2001**, *35*, 2060−2072.
(38) Kim, E.; Hopke, P. K.; Larson, T. V.; Maykut, N. N.; Lewtas, J. Factor analysis of Seattle fine particles. *Aerosol Sci. Technol.* **2004**, *38*, 724−738.
(39) Owega, S.; Khan, B. U. Z.; D'Souza, R.; Evans, G. J.; Fila, M.; Jervis, R. E. Receptor modeling of Toronto PM2.5 characterized by aerosol laser ablation mass spectrometry. *Environ. Sci. Technol.* **2004**, *38*, 5712−5720.
(40) Sodeman, D. A.; Toner, S. M.; Shields, L. G.; Suess, D. T.; Gross, D. S.; Prather, K. A. Comparison of light duty and heavy duty vehicle emissions from dynamometer and tunnel studies using ART-2a. Manuscript in preparation.
(41) Silva, P. J.; Liu, D. Y.; Noble, C. A.; Prather, K. A. Size and chemical characterization of individual particles resulting from biomass burning of local Southern California species. *Environ. Sci. Technol.* **1999**, *33*, 3068−3076.
(42) Suess, D. T.; Prather, K. A. Reproducibility of single particle chemical composition during a heavy duty diesel truck dynamometer study. *Aerosol Sci. Technol.* **2002**, *36*, 1139−1141.
(43) Shields, L. G.; Suess, D. T.; Guazzotti, S. A.; Prather, K. A. Determination of single particle mass spectral signatures from heavy duty vehicle emissions. Manuscript in preparation.
(44) Song, X. H.; Faber, N. M.; Hopke, P. K.; Suess, D. T.; Prather, K. A.; Schauer, J. J.; Cass, G. R. Source apportionment of gasoline and diesel by multivariate calibration based on single particle mass spectral data. *Anal. Chim. Acta* **2001**, *446*, 329−343.
(45) Toner, S. M.; Sodeman, D. A. Prather, K. A. Single particle characterization of ultrafine and accumulation mode particles from heavy duty diesel vehicles using aerosol time-of-flight mass spectrometry. Manuscript in preparation.
(46) Hildemann, L. M.; Cass, G. R.; Markowski, G. R. A dilution stack sampler for collection of organic aerosol emissions: Design, characterization and field-tests. *Aerosol. Sci. Technol.* **1989**, *10*, 193−204.
(47) Robert, M. A.; Jakober, C. A.; VanBergen, S.; Kleeman, M. J. Size and composition distributions of particulate matter emissions 1. Light duty gasoline vehicles. Manuscript in preparation.
(48) Su, Y. X.; Sipin, M. F.; Furutani, H.; Prather, K. A. Development and characterization of an aerosol time-of-flight mass spectrometer with increased detection efficiency. *Anal. Chem.* **2004**, *76*, 712−719.
(49) Gard, E.; Mayer, J. E.; Morrical, B. D.; Dienes, T.; Fergenson, D. P.; Prather, K. A. Real-time analysis of individual atmospheric

aerosol particles: Design and performance of a portable ATOFMS. *Anal. Chem.* **1997**, *69*, 4083−4091.
(50) Allen, J. O.; Fergenson, D. P.; Gard, E. E.; Hughes, L. S.; Morrical, B. D.; Kleeman, M. J.; Gross, D. S.; Galli, M. E.; Prather, K. A.; Cass, G. R. Particle detection efficiencies of aerosol time of flight mass spectrometers under ambient sampling conditions. *Environ. Sci. Technol.* **2000**, *34*, 211−217.
(51) Wenzel, R. J.; Liu, D. Y.; Edgerton, E.; Prather, K. A. Aerosol time-of-flight mass spectrometry during the Atlanta Supersite Experiment: 2. Scaling procedures. *J. Geophys. Res., Atmos.* **2003**, *108*, 8427.
(52) Van Gulijk, C.; Marijnissen, J. C. M.; Makkee, M.; Moulijn, J. A.; Schmidt-Ott, A. Measuring diesel soot with a scanning mobility particle sizer and an electrical low-pressure impactor: performance assessment with a model for fractal-like agglomerates. *J. Aerosol Sci.* **2004**, *35*, 633−655.
(53) DeCarlo, P.; Slowik, J. G.; Worsnop, D. R.; Davidovits, P.; Jimenez, J. L. Particle Morphology and Density Characterization by Combined Mobility and Aerodynamic Diameter Measurements. Part 1: Theory. *Aerosol Sci. Technol.* **2004**, *38*, 1185−1205.
(54) Slowik, J. G.; Stainken, K.; Davidovits, P.; Williams, L. R.; Jayne, J. T.; Kolb, C. E.; Worsnop, D. R.; Rudich, Y.; DeCarlo, P.; Jimenez, J. L. Particle morphology and density characterization by combined mobility and aerodynamic diameter measurements. Part 2: Application to combustion-generated soot aerosols as a function of fuel equivalence ratio. *Aerosol Sci. Technol.* **2004**, *38*, 1206−1222.
(55) Dahneke, B. Aerosol beams. In *Recent Developments in Aerosol Science*; Shaw, D., Ed.; Wiley: New York, 1976.
(56) Bein, K. J.; Zhao, Y.; Wexler, A. S.; Johnston, M. V. Speciation of size-resolved individual ultrafine particles in Pittsburgh, Pennsylvania. *J. Geophys. Res.* **2005**, *110*, D07S05; doi: 10.1029/2004JD004708.
(57) Spencer, M. T.; Shields, L. G.; Sodeman, D. A.; Toner, S. M.; Suess, D. T.; Prather, K. A. Comparison of oil and fuel aerosol chemical signatures with heavy duty and light duty vehicle emissions using ATOFMS. Manuscript in preparation.
(58) Song, X. H.; Hopke, P. K.; Fergenson, D. P.; Prather, K. A. Classification of single particles analyzed by ATOFMS using an artificial neural network, ART-2A. *Anal. Chem.* **1999**, *71*, 860−865.
(59) Phares, D. J.; Rhoads, K. P.; Wexler, A. S.; Kane, D. B.; Johnston, M. V. Application of the ART-2a algorithm to laser ablation aerosol mass spectrometry of particle standards. *Anal. Chem.* **2001**, *73*, 2338−2344.
(60) Liu, D. Y.; Wenzel, R. J.; Prather, K. A. Aerosol time-of-flight mass spectrometry during the Atlanta Supersite experiment: 1. Measurements. *J. Geophys. Res., Atmos.* **2003**, *108*, 8426.
(61) Bhave, P. V.; Allen, J. O.; Morrical, B. D.; Fergenson, D. P.; Cass, G. R.; Prather, K. A. A field-based approach for determining ATOFMS instrument sensitivities to ammonium and nitrate. *Environ. Sci. Technol.* **2002**, *36*, 4868−4879.
(62) Willermet, P. A. Some engine oil additives and their effects on antiwear film formation. *Tribol. Lett.* **1998**, *5*, 41−47.
(63) Yamaguchi, E. S.; Roby, S. H.; Francisco, M. M.; Ruelas, S. G.; Godfrey, D. Antiwear film formation by ZnDTP, detergent, and dispersant components of passenger car motor oils. *Tribol. Trans.* **2002**, *45*, 425−429.
(64) Rizvi, S. Q. Dispersants. In *Lubricant Additives: Chemistry and Applications*; Rudnick, L. R., Ed.; Marcel Dekker: New York, 2002; pp 137−170.
(65) Sakurai, H.; Tobias, H. J.; Park, K.; Zarling, D.; Docherty, S.; Kittelson, D. B.; McMurry, P. H.; Ziemann, P. J. On-line measurements of diesel nanoparticle composition and volatility. *Atmos. Environ.* **2003**, *37*, 1199−1210.
(66) Harrison, R. M.; Tilling, R.; Romero, M. S. C.; Harrad, S.; Jarvis, K. A study of trace metals and polycyclic aromatic hydrocarbons in the roadside environment. *Atmos. Environ.* **2003**, *37*, 2391−2402.
(67) Singh, M.; Jaques, P. A.; Sioutas, C. Size distribution and diurnal characteristics of particle-bound metals in source and receptor sites of the Los Angeles Basin. *Atmos. Environ.* **2002**, *36*, 1675−1689.
(68) Vogt, R.; Kirchner, U.; Scheer, V.; Hinz, K. P.; Trimborn, A.; Spengler, B. Identification of diesel exhaust particles at an Autobahn, urban and rural location using single-particle mass spectrometry. *J. Aerosol Sci.* **2003**, *34*, 319−337.
(69) Gross, D. S.; Galli, M. E.; Silva, P. J.; Prather, K. A. Relative sensitivity factors for alkali metal and ammonium cations in single particle aerosol time-of-flight mass spectra. *Anal. Chem.* **2000**, *72*, 416−422.
(70) Wenzel, R. J.; Prather, K. A. Improvements in ion signal reproducibility obtained using a homogeneous laser beam for on-line laser desorption/ionization of single particles. *Rapid Commun. Mass Spectrom.* **2004**, *18*, 1525−1533.
(71) Fraser, M. P.; Cass, G. R. Detection of excess ammonia emissions from in-use vehicles and the implications for fine particle control. *Environ. Sci. Technol.* **1998**, *32*, 1053−1057.
(72) McLafferty, F. W.; Tureécek, F. *Interpretation of mass spectra*, 4th ed.; University Science Books: Mill Valley, CA, 1993.
(73) Cadle, S. H.; Mulawa, P.; Groblicki, P.; Laroo, C.; Ragazzi, R. A.; Nelson, K.; Gallagher, G.; Zielinska, B. In-use light-duty gasoline vehicle particulate matter emissions on three driving cycles. *Environ. Sci. Technol.* **2001**, *35*, 26−32.
(74) Marr, L. C.; Kirchstetter, T. W.; Harley, R. A.; Miguel, A. H.; Hering, S. V.; Hammond, S. K. Characterization of polycyclic aromatic hydrocarbons in motor vehicle fuels and exhaust emissions. *Environ. Sci. Technol.* **1999**, *33*, 3091−3099.
(75) Wang, J.; Jia, C. R.; Wong, C. K.; Wong, P. K. Characterization of polycyclic aromatic hydrocarbons created in lubricating oils. *Water, Air, Soil Pollut.* **2000**, *120*, 381−396.
(76) Miguel, A. H.; Kirchstetter, T. W.; Harley, R. A.; Hering, S. V. On-road emissions of particulate polycyclic aromatic hydrocarbons and black carbon from gasoline and diesel vehicles. *Environ. Sci. Technol.* **1998**, *32*, 450−455.
(77) Pereira, P. A. D.; de Andrade, J. B.; Miguel, A. H. Measurements of semivolatile and particulate polycyclic aromatic hydrocarbons in a bus station and an urban tunnel in Salvador, Brazil. *J. Environ. Monit.* **2002**, *4*, 558−561.
(78) Venkataraman, C.; Lyons, J. M.; Friedlander, S. K. Size distributions of polycyclic aromatic hydrocarbons and elemental carbon 1: Sampling, measurement methods, and source characterization. *Environ. Sci. Technol.* **1994**, *28*, 555−562.
(79) Wingfors, H.; Sjodin, A.; Haglund, P.; Brorstrom-Lunden, E. Characterization and determination of profiles of polycyclic aromatic hydrocarbons in a traffic tunnel in Gothenburg, Sweden. *Atmos. Environ.* **2001**, *35*, 6361−6369.
(80) Odum, J. R.; Jungkamp, T. P. W.; Griffin, R. J.; Flagan, R. C.; Seinfeld, J. H. The atmospheric aerosol-forming potential of whole gasoline vapor. *Science* **1997**, *276*, 96−99.
(81) Divita, F.; Ondov, J. M.; Suarez, A. E. Size spectra and atmospheric growth of V-containing aerosol in Washington, DC. *Aerosol Sci. Technol.* **1996**, *25*, 256−273.
(82) Barceloux, D. G. Vanadium. *J. Toxicol., Clin. Toxicol.* **1999**, *37*, 265−278.
(83) Sabbioni, E.; Kueera, J.; Pietra, R.; Vesterberg, O. A critical review on normal concentrations of vanadium in human blood, serum, and urine. *Sci. Total Environ.* **1996**, *188*, 49−58.
(84) Tolocka, M. P.; Lake, D. A.; Johnston, M. V.; Wexler, A. S. Number concentrations of fine and ultrafine particles containing metals. *Atmos. Environ.* **2004**, *38*, 3263−3273.
(85) Noble, C. A.; Prather, K. A. Real-time measurement of correlated size and composition profiles of individual atmospheric aerosol particles. *Environ. Sci. Technol.* **1996**, *30*, 2667−2680.
(86) Watson, J. G.; Chow, J. C.; Lowenthal, D. H.; Pritchett, L. C.; Frazier, C. A.; Neuroth, G. R.; Robbins, R. Differences in the carbon composition of source profiles for diesel-powered and gasoline-powered vehicles. *Atmos. Environ.* **1994**, *28*, 2493−2505.
(87) Spencer, M. T.; Prather, K. A. Quantification of the fraction of organic carbon elemental carbon particles using single particle mass spectrometry. Manuscript in preparation.
(88) Schauer, J. J.; Mader, B. T.; Deminter, J. T.; Heidemann, G.; Bae, M. S.; Seinfeld, J. H.; Flagan, R. C.; Cary, R. A.; Smith, D.; Huebert, B. J.; Bertram, T.; Howell, S.; Kline, J. T.; Quinn, P.; Bates, T.; Turpin, B.; Lim, H. J.; Yu, J. Z.; Yang, H.; Keywood, M. D. ACE-Asia intercomparison of a thermal-optical method for the determination of particle-phase organic and elemental carbon. *Environ. Sci. Technol.* **2003**, *37*, 993−1001.
(89) Chow, J. C.; Watson, J. G.; Crow, D.; Lowenthal, D. H.; Merrifield, T. Comparison of IMPROVE and NIOSH carbon measurements. *Aerosol Sci. Technol.* **2001**, *34*, 23−34.
(90) Su, Y. X.; Sipin, M. F.; Spencer, M. T.; Qin, X.; Moffet, R. C.; Shields, L. G.; Gupta, T.; Demokritou, P.; Koutrakis, P.; Venkatachari, P.; Jeong, C. H.; Kim, E.; Hopke, P. K.; Gelein, R. M.; Utell, M. J.; Oberdorster, G.; Bernsten, J.; Delvin, R.; Chen, L. C.; Prather, K. A. Real-time characterization of the composition of individual particles emitted from particle concentrators. Submitted to *Aerosol Sci. Technol.*
(91) Ristovski, Z. D.; Morawska, L.; Bofinger, N. D.; Hitchins, J. Submicrometer and supermicrometer particulate emission from spark ignition vehicles. *Environ. Sci. Technol.* **1998**, *32*, 3845−3852.

(92) Kristensson, A.; Johansson, C.; Westerholm, R.; Swietlicki, E.; Gidhagen, L.; Wideqvist, U.; Vesely, V. Real-world traffic emission factors of gases and particles measured in a road tunnel in Stockholm, Sweden. *Atmos. Environ.* **2004**, *38*, 657−673.
(93) Ketzel, M.; Wahlin, P.; Berkowicz, R.; Palmgren, F. Particle and trace gas emission factors under urban driving conditions in Copenhagen based on street and roof-level observations. *Atmos. Environ.* **2003**, *37*, 2735−2749.
(94) Jamriska, M.; Morawska, L. A model for determination of motor vehicle emission factors from on-road measurements with a focus on submicrometer particles. *Sci. Total Environ.* **2001**, *264*, 241−255.
(95) Gramotnev, G.; Brown, R.; Ristovski, Z.; Hitchins, J.; Morawska, L. Determination of average emission factors for vehicles on a busy road. *Atmos. Environ.* **2003**, *37*, 465−474.
(96) Farrauto, R. J.; Heck, R. M. Catalytic converters: State of the art and perspectives. *Catal. Today* **1999**, *51*, 351−360.
(97) Heck, R. M.; Farrauto, R. J. Automobile exhaust catalysts. *Appl. Catal., A* **2001**, *221*, 443−457.
(98) Kaspar, J.; Fornasiero, P.; Hickey, N. Automotive catalytic converters: Current status and some perspectives. *Catal. Today* **2003**, *77*, 419−449.
(99) Bishop, G. A.; Stedman, D. H. Measuring the emissions of passing cars. *Acc. Chem. Res.* **1996**, *29*, 489−495.
(100) Seagrave, J.; McDonald, J. D.; Gigliotti, A. P.; Nikula, K. J.; Seilkop, S. K.; Gurevich, M.; Mauderly, J. L. Mutagenicity and in vivo toxicity of combined particulate and semivolatile organic fractions of gasoline and diesel engine emissions. *Toxicol. Sci.* **2002**, *70*, 212−226.
(101) Bezabeh, D. Z.; Allen, T. M.; McCauley, E. M.; Kelly, P. B.; Jones, A. D. Negative ion laser desorption ionization time-of-flight mass spectrometry of nitrated polycyclic aromatic hydrocarbons. *J. Am. Soc. Mass. Spectrom.* **1997**, *8*, 630−636.
(102) Durant, J. L.; Busby, W. F.; Lafleur, A. L.; Penman, B. W.; Crespi, C. L. Human cell mutagenicity of oxygenated, nitrated and unsubstituted polycyclic aromatic hydrocarbons associated with urban aerosols. *Mutat. Res. Genetic Toxicol.* **1996**, *371*, 123−157.
(103) Yaffe, D.; Cohen, Y.; Arey, J.; Grosovsky, A. J. Multimedia analysis of PAHs and nitro-PAH daughter products in the Los Angeles basin. *Risk Anal.* **2001**, *21*, 275−294.
(104) Dimashki, M.; Harrad, S.; Harrison, R. M. Measurements of nitro-PAH in the atmospheres of two cities. *Atmos. Environ.* **2000**, *34*, 2459−2469.
(105) Hayakawa, K.; Murahashi, T.; Akutsu, K.; Kanda, T.; Tang, N.; Kakimoto, H.; Toriba, A.; Kizu, R. Comparison of polycyclic aromatic hydrocarbons and nitropolycyclic aromatic hydrocarbons in airborne and automobile exhaust particulates. *Polycyclic Aromat. Compd.* **2000**, *20*, 179−190.

Received for review July 1, 2004. Revised manuscript received March 1, 2005. Accepted April 5, 2005.